Ab initio investigation of OH vehicle migration in yttrium-doped barium zirconate

Article Supplement

Sebastian Eisele[a], Jan N. Andreschak[a], Fabian M. Draber[a], Manfred Martin[a], Steffen Neitzel-Grieshammer[b]*

[a] Institute of Physical Chemistry, RWTH Aachen University, Landoltweg 2, 52074 Aachen, Germany.
[b] Department of Chemical Engineering, FH Münster University of Applied Sciences, Stegerwaldstr. 39, 48565 Steinfurt, Germany
* Correspondence to: Steffen Neitzel-Grieshammer, steffen.neitzel-grieshammer@fh-muenster.de

Abstract

This supplement contains additional information and results for the main article "*Ab initio investigation of OH vehicle migration in yttrium-doped barium zirconate*". The geometric description of all used transition for the KMC simulations are presented as well as the full energetic model definition including pair interactions and base barrier configurations. The migration energy distributions of each process simulated with KMC at 1273 K are shown.

Kinetic Monte Carlo event description

The kinetic Monte Carlo (KMC) transition data is defined according to the MOCASSIN state change system that uses transition rules bound to reference geometries which are then symmetry extended by the framework (see refs.[1,2]). In this formalism, the three occurring states $S_{\text{initial}}, S_{\text{trans}}, S_{\text{final}}$ of the oxygen vacancy 1NN migration (O-T) and proton hopping processes (H-T, H-R) are defined according to the matrix notation in eq. (1).

$$\begin{bmatrix} & p_0 & p_1 & p_2 \\ S_{\text{initial}} & \text{H}_\text{i}^\bullet & \emptyset & \text{V}_\text{i}^\times \\ S_{\text{trans}} & \emptyset & \text{H}_\emptyset^\bullet & \emptyset \\ S_{\text{final}} & \text{V}_\text{i}^\times & \emptyset & \text{H}_\text{i}^\bullet \end{bmatrix} \qquad \begin{bmatrix} & p_0 & p_1 & p_2 \\ S_{\text{initial}} & \text{O}_\text{O}^\times & \emptyset & \text{V}_\text{O}^{\bullet\bullet} \\ S_{\text{trans}} & \emptyset & \text{O}_\emptyset'' & \emptyset \\ S_{\text{final}} & \text{V}_\text{O}^{\bullet\bullet} & \emptyset & \text{O}_\text{O}^\times \end{bmatrix} \tag{1}$$

Here, the involved position of the transition path – the matrix columns – are indexed as $p_0, \dots, p_n$. The $\emptyset$ symbol marks the non-interacting *VOID* occupation of a position that is neither particle nor vacancy, which is the standard occupation for unstable transition positions. The species $\text{H}_\emptyset^\bullet$ and $\text{O}_\emptyset''$ describe a proton or oxygen located at the unstable transition position. Due to a *detailed balance*, both processes can also be executed in reverse, that is, S_{initial} and S_{final} are interchangeable. The binding geometries, that is, the reference transition paths, for the rules are summarized in table 1 alongside their labels in the main article and the number of symmetry equivalent events per unit cell and site. The symmetry extension is done with the 48 symmetry operations of space group $Pm\bar{3}m$.

Table 1 Reference event geometries for the proton and oxygen hopping mechanisms in BZY as required for the MOCASSIN input using a unit cell definition according to the main article.

Transition	Label in main article	Unique paths per cell/site	MOCASSIN Binding geometry
Oxygen migration	O-T	24/8	$\begin{bmatrix} & x & y & z \\ p_0 & 0.5 & 0 & 0 \\ p_1 & 0.75 & 0.25 & 0 \\ p_2 & 1 & 0.25 & 0 \end{bmatrix}$
Proton translation	H-T	24/2	$\begin{bmatrix} & x & y & z \\ p_0 & 0.5 & 0.2364 & 0 \\ p_1 & 0.6318 & 0.3682 & 0 \\ p_2 & 0.7636 & 0.5 & 0 \end{bmatrix}$
Proton reorientation	H-R	24/2	$\begin{bmatrix} & x & y & z \\ p_0 & 0.5 & 0.2364 & 0 \\ p_1 & 0.5 & 0.1182 & 0.1182 \\ p_2 & 0.5 & 0 & 0.2364 \end{bmatrix}$

The binding geometries of the vehicle cases are constructed as two consecutive regular migrations – first oxygen then proton migration, since the oxygen ion is supposed to be the event origin point – where instead of the two transition positions a single unified transition position that is occupied by an $\text{OH}_\emptyset'$ species during the transition state is used. Thus, each transition path has the positions $p_0, \dots, p_4$ where p_2 is the unstable transition position. The affiliated transition rule notation that is

valid for both translation and dissociation cases is given in eq. (2). Again an inverted rule that interchanges S_{initial} and S_{final} exists.

$$\begin{bmatrix} & p_0 & p_1 & p_2 & p_3 & p_4 \\ S_{\text{initial}} & \text{O}_\text{O}^\times & \text{V}_\text{O}^{\bullet\bullet} & \emptyset & \text{H}_\text{i}^\bullet & \text{V}_\text{i}^\times \\ S_{\text{trans}} & \emptyset & \emptyset & \text{OH}_\emptyset' & \emptyset & \emptyset \\ S_{\text{final}} & \text{V}_\text{O}^{\bullet\bullet} & \text{O}_\text{O}^\times & \emptyset & \text{V}_\text{i}^\times & \text{H}_\text{i}^\bullet \end{bmatrix} \tag{2}$$

Due to performance optimizations of the KMC algorithm, only the minority species $\text{H}_\text{i}^\bullet$ and $\text{V}_\text{O}^{\bullet\bullet}$ are selected as event origin points. Hence, only the inverted required binding geometry can be chosen during simulation. Vehicle translations should be executed forward and backwards while vehicle dissociations should not be executed backwards since the occurrence of association events must be prevented unless specifically defined as another transition. Accordingly, the binding geometries for the four vehicle transitions are chosen such that executing only the inverted rule of eq. (2) leads to the described behavior execution options for all processes. The affiliated geometric data is summarized in table 2.

Table 2 Reference event geometries for the vehicle translation and dissociation mechanisms in BZY as required for the MOCASSIN input using a unit cell definition according to the main article.

Transition	Label in main article	Unique paths per cell/site	MOCASSIN Binding geometry
Vehicle 2-5 translation	OH-T-2-5	48/16	$\begin{bmatrix} & x & y & z \\ p_0 & 0.5 & 0 & 0 \\ p_1 & 1 & 0.5 & 0 \\ p_2 & 0.75 & 0.25 & 0 \\ p_3 & 0.5 & 0 & 0.2364 \\ p_4 & 1 & 0.5 & 0.2364 \end{bmatrix}$
Vehicle 3-4 translation	OH-T-3-4	24/8	$\begin{bmatrix} & x & y & z \\ p_0 & 0.5 & 0 & 0 \\ p_1 & 1 & 0.5 & 0 \\ p_2 & 0.75 & 0.25 & 0 \\ p_3 & 0.5 & 0.2364 & 0 \\ p_4 & 0.7636 & 0.5 & 0 \end{bmatrix}$
Vehicle 2-5 dissociation	OH-D-2-5	48/16	$\begin{bmatrix} & x & y & z \\ p_0 & 1 & 0.5 & 0 \\ p_1 & 0.5 & 0 & 0 \\ p_2 & 0.75 & 0.25 & 0 \\ p_3 & 0.7636 & 0 & 0.5 \\ p_4 & 0.5 & 0 & 0.2364 \end{bmatrix}$
Vehicle 3-4 dissociation	OH-D-3-4	24/8	$\begin{bmatrix} & x & y & z \\ p_0 & 1 & 0.5 & 0 \\ p_1 & 0.5 & 0 & 0 \\ p_2 & 0.75 & 0.25 & 0 \\ p_3 & 0.2364 & 0.5 & 0 \\ p_4 & 0.5 & 0.2364 & 0 \end{bmatrix}$

Additional kinetic Monte Carlo interaction data

The pair interaction data and cluster configurations for vehicle transitions can be found in the main article. This section contains the missing cluster configurations and base barriers ΔE_{base} for the proton and oxygen vacancy hopping not contained in the main article. The data for the transitions O-T, H-T, and H-R are summarized in

table 3, table 4, and table 5, respectively. Note that as explained in the main article, the three-body configuration of the Zr positions has two C_2 symmetric cases where the asymmetry of the energy for forward/backward jump is implicitly achieved by the pair interactions. This is relevant for the O-T and H-T migration geometries where the DFT migration barriers of refs.[3–5] cannot be mapped exactly to the state-based energy modelling approach used by the MOCASSIN framework. The C_2 symmetry axis for the two-body configuration of the H-R transition is perpendicular to the migration vector, thus there is no energetic asymmetry for forward and backward movement directions.

Table 3 Cluster configuration and base barriers of O-T 1NN oxygen vacancy hopping. Zirconium is in green, and yttrium is in blue. Values marked with (*) have a C_2 symmetric counter part with the same energy. The data is based on refs.[4,5].

Configuration	ΔE_{base} / eV	Configuration	ΔE_{base} / eV
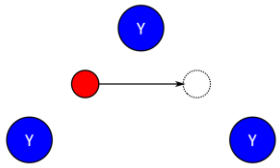	0.88	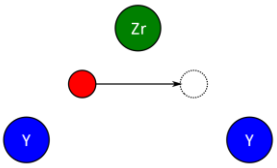	0.64
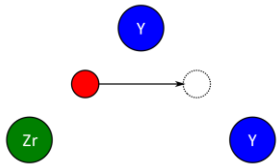	*0.91	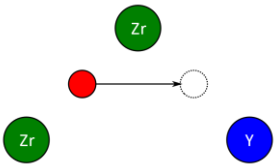	*0.59
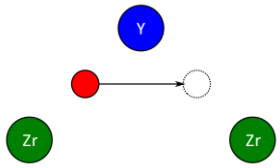	1.16	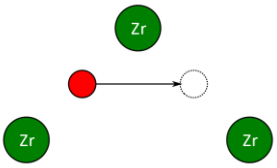	0.66

Table 4 Cluster configuration and base barriers of H-T proton translation. Zirconium is in green, and yttrium is in blue. Values marked with (*) have a C_2 symmetric counter part with the same energy. The data is based on refs.[3,5].

Configuration	ΔE_{base} / eV	Configuration	ΔE_{base} / eV
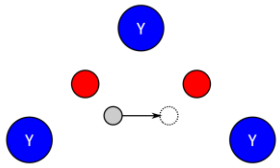	0.66	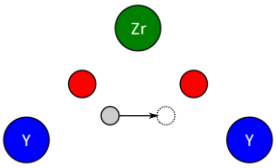	0.55
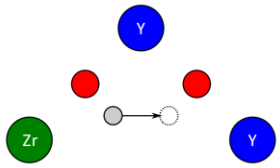	*0.37	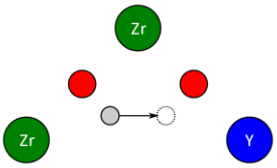	*0.35
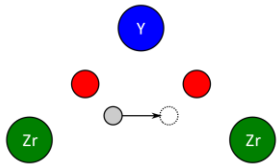	0.22	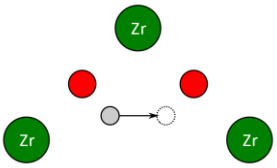	0.41

Table 5 Cluster configuration and base barriers of H-R proton reorientation. Zirconium is in green, and yttrium is in blue. Values marked with (*) have a C_2 symmetric counter part with the same energy. The data is based on refs.[3,5].

Configuration	ΔE_{base} / eV	Configuration	ΔE_{base} / eV
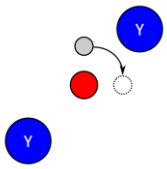	0.13	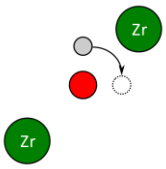	0.15
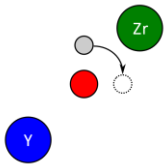	*0.22		

Migration barrier distributions of BZY10 from KMC

The energy barrier distributions shown in figure to figure illustrate the fraction of barriers occurred during jump attempts of the specified transition type alongside the fraction of MCS actually performed at those barriers. The jump attempt fraction $f_m(E)$ and MCS fraction $f_{m,\mathrm{MCS}}(E)$ for a transition type m as a function of the energy E are calculated according to eqs. (3) and (4), respectively. Here, $N_m(E)$ is the number of attempts of transition type m that occurred at migration barrier energy E, k_B is the Boltzmann factor, and T is the temperature. All shown distributions were recorded with a single simulation at $T = 1273$ K and contain the data from 1000 – 2000 Monte Carlo steps per mobile particle, that is, each distribution contains the data from several hundred million transition attempts.

$$f_m(E) = \frac{N_m(E)}{\int_0^\infty N_m(E)\mathrm{d}E} \tag{3}$$

$$f_{m,\mathrm{MCS}}(E) = \frac{N_m(E)\exp\left(-\frac{E}{k_\mathrm{B}T}\right)}{\int_0^\infty N_m(E)\exp\left(-\frac{E}{k_\mathrm{B}T}\right)\mathrm{d}E} \tag{4}$$

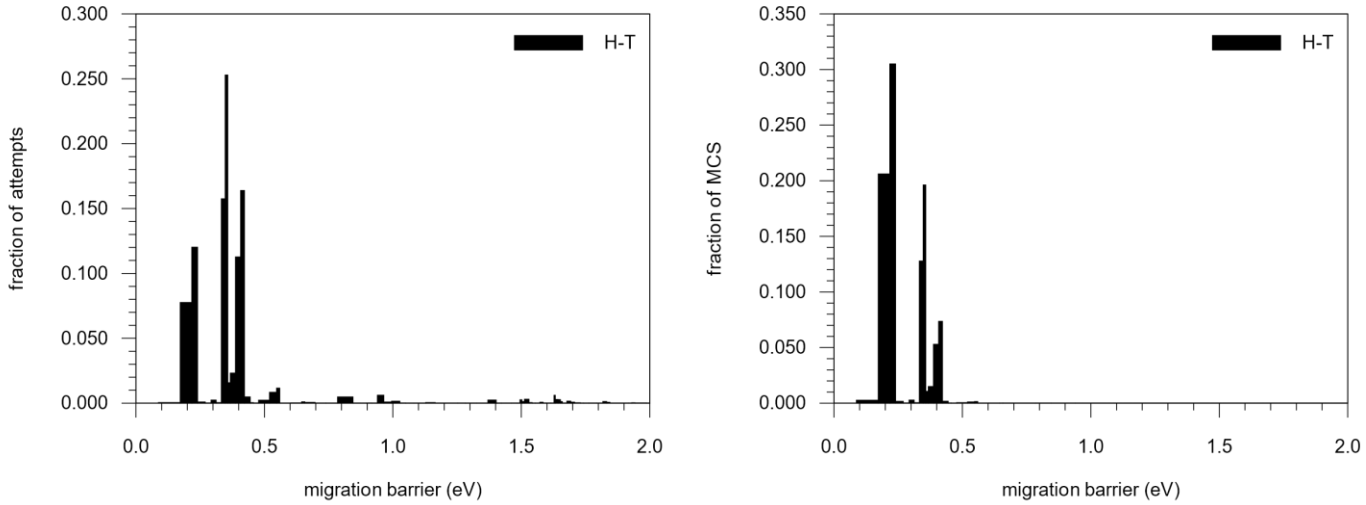

Figure 1 Migration barrier energy distribution of all transitions attempts (left) and successful Monte Carlo steps (right) of the H-T transition in BZY10 at a degree of hydration of 50% and 1273 K as simulated with KMC. The data is normalized to the total number of attempts/MCS executed for this transition type and values above 2 eV are not shown.

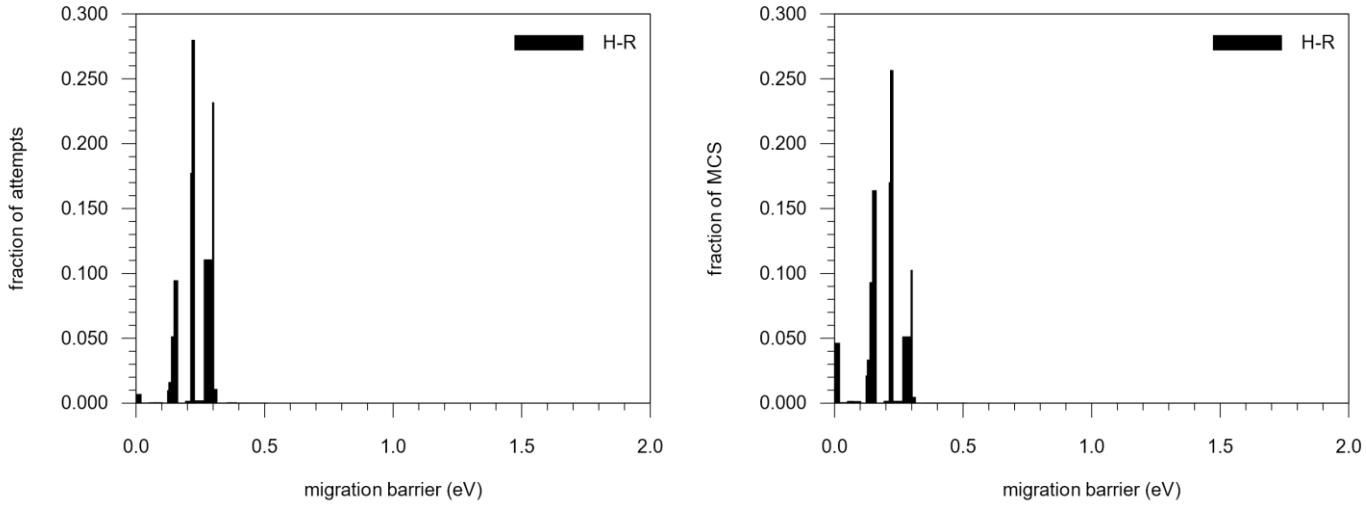

Figure 2 Migration barrier energy distribution of all transitions attempts (left) and successful Monte Carlo steps (right) of the H-R transition in BZY10 at a degree of hydration of 50% and 1273 K as simulated with KMC. The data is normalized to the total number of attempts/MCS executed for this transition type and values above 2 eV are not shown.

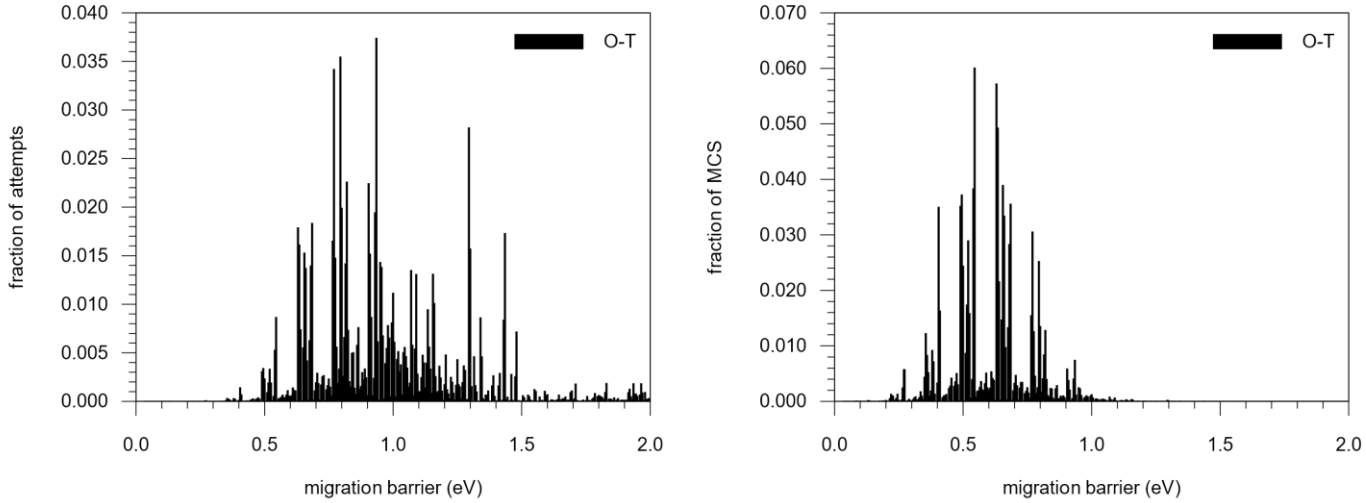

Figure 3 Migration barrier energy distribution of all transitions attempts (left) and successful Monte Carlo steps (right) of the O-T transition in BZY10 at a degree of hydration of 50% and 1273 K as simulated with KMC. The data is normalized to the total number of attempts/MCS executed for this transition type and values above 2 eV are not shown.

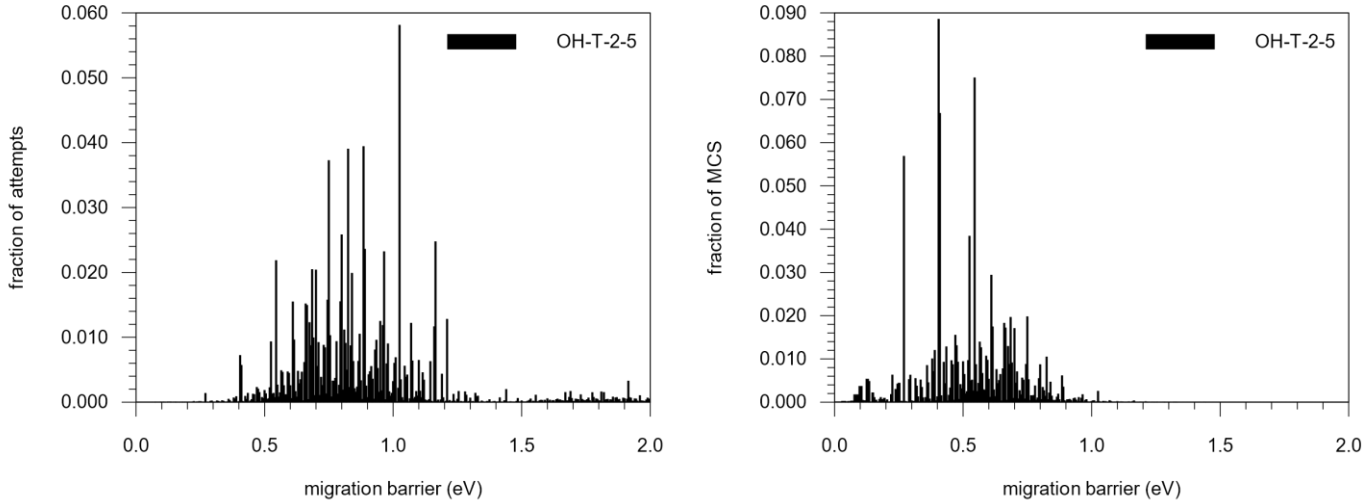

Figure 4 Migration barrier energy distribution of all transitions attempts (left) and successful Monte Carlo steps (right) of the OH-T-2-5 transition in BZY10 at a degree of hydration of 50% and 1273 K as simulated with KMC. The data is normalized to the total number of attempts/MCS executed for this transition type and values above 2 eV are not shown.

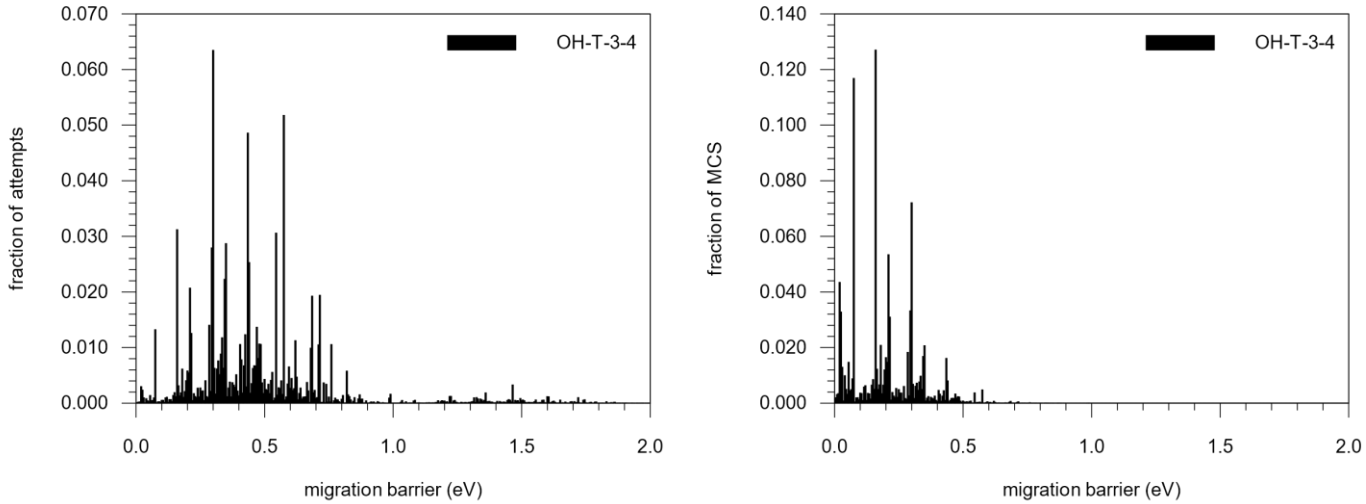

Figure 5 Migration barrier energy distribution of all transitions attempts (left) and successful Monte Carlo steps (right) of the OH-T-3-4 transition in BZY10 at a degree of hydration of 50% and 1273 K as simulated with KMC. The data is normalized to the total number of attempts/MCS executed for this transition type and values above 2 eV are not shown.

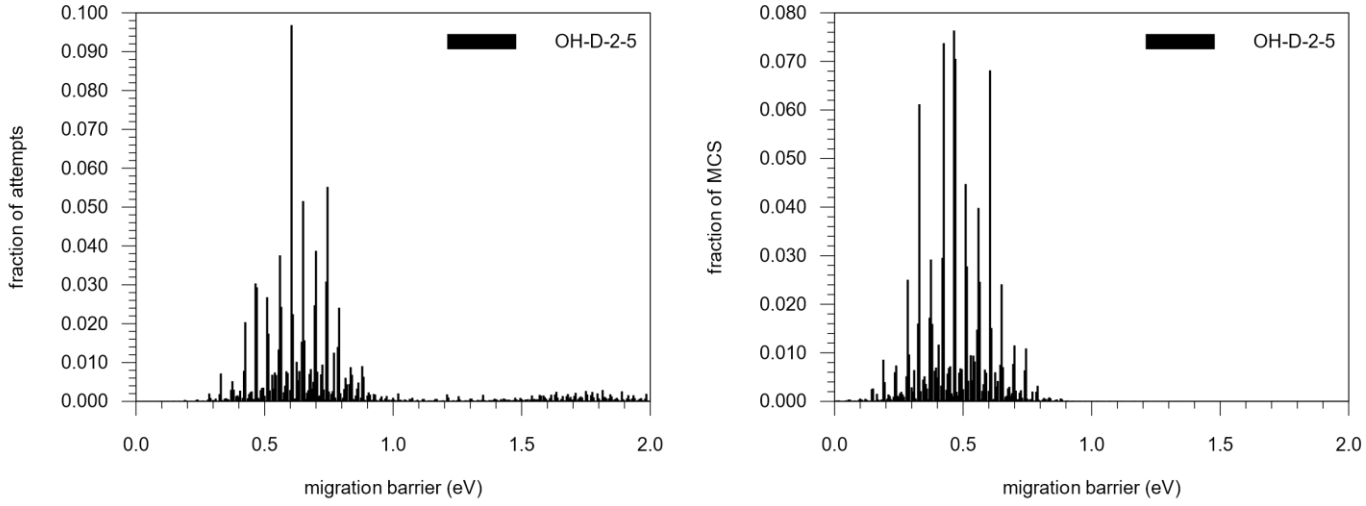

Figure 6 Migration barrier energy distribution of all transitions attempts (left) and successful Monte Carlo steps (right) of the OH-D-2-5 transition in BZY10 at a degree of hydration of 50% and 1273 K as simulated with KMC. The data is normalized to the total number of attempts/MCS executed for this transition type and values above 2 eV are not shown.

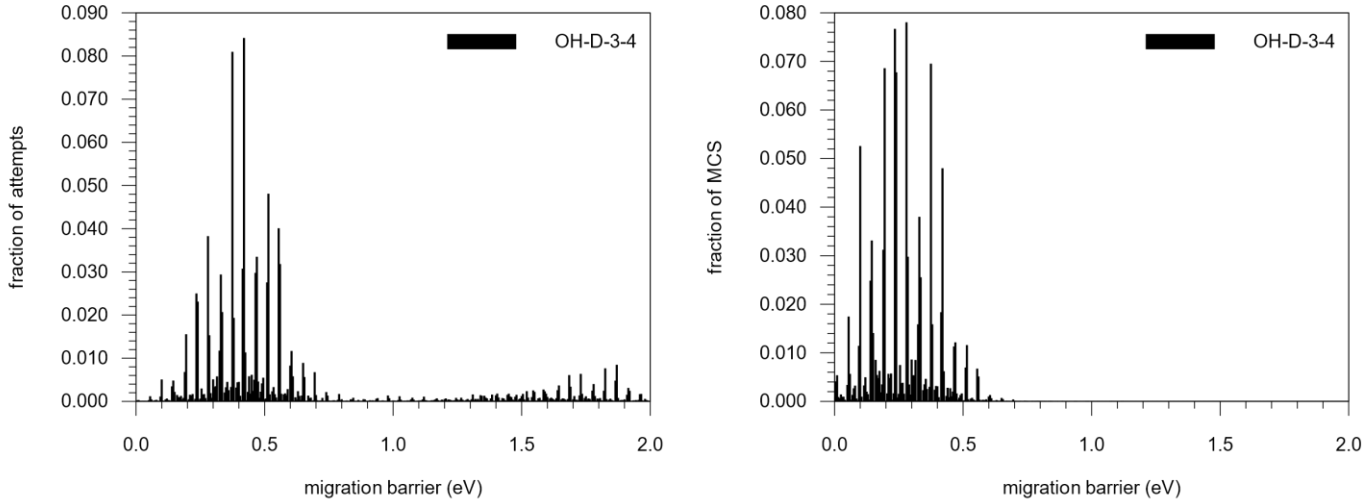

Figure 7 Migration barrier energy distribution of all transitions attempts (left) and successful Monte Carlo steps (right) of the OH-D-3-4 transition in BZY10 at a degree of hydration of 50% and 1273 K as simulated with KMC. The data is normalized to the total number of attempts/MCS executed for this transition type and values above 2 eV are not shown.

Effect of electric field

An electric field is applied in the simulations to obtain the ionic conductivity. Figure 8 shows the simulated conductivity depending on the applied field for oxide ions in BZO10 with $\beta = 0.5$ at 1000 K. The chosen field strength of 10^7 V/m is well within the linear regime. At significantly stronger fields the conductivity becomes field-dependent while significantly weaker fields result in poor statistical quality.

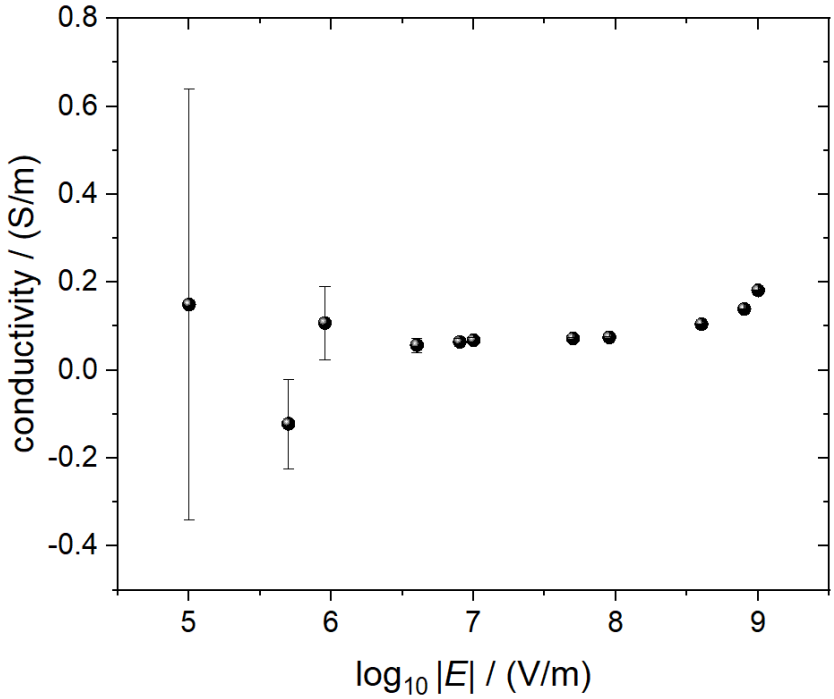

Figure 8 Displacement of protons in the electric field for BZO10 with $\beta = 0.5$, including the vehicle mechanism. Displacement is shown depending on the number of Monte Carlo steps per particle (MCSP) which is proportional to the simulated time.

Displacement plots for oxide ions and protons

The ionic conductivity and mobility is obtained from the mean displacement of ions in the applied electric field. The figures show the displacement of protons (Figure 9) and oxide ions (Figure 10) for BZO10 with $\beta = 0.5$ including the vehicle mechanism at different temperatures. For the sake of representation, displacements are plotted depending on the number of Monte Carlo steps per particle (MCSP) which is proportional to the simulated time for each temperature. All plots show the expected linear behavior. The only exception are oxide ions at 773 K where more fluctuation is observed. This is reflected in larger relative errors in the computed conductivities.

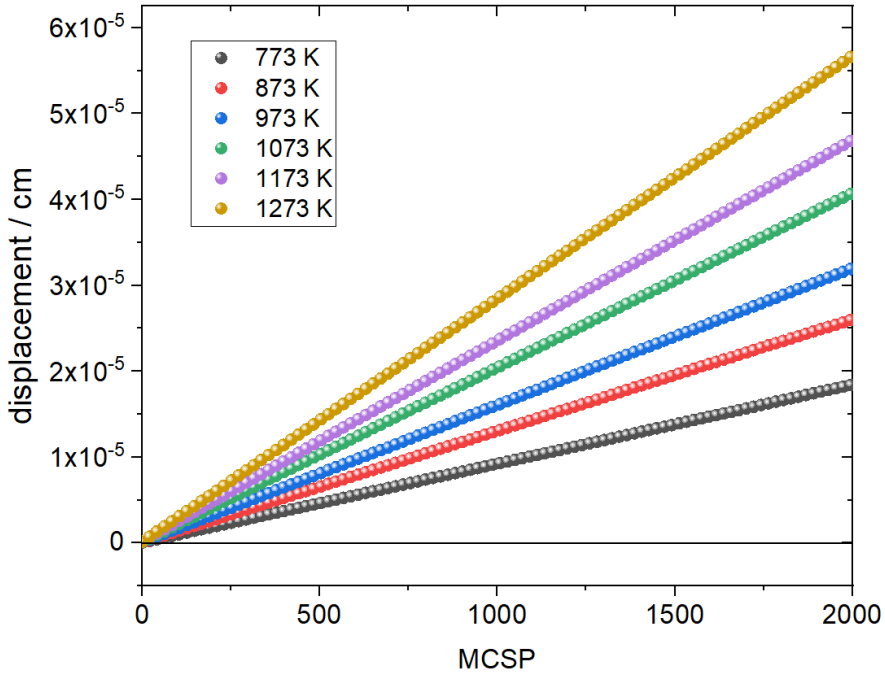

Figure 9 Displacement of protons in the electric field for BZO10 with $\beta = 0.5$, including the vehicle mechanism. Displacement is shown depending on the number of Monte Carlo steps per particle (MCSP) which is proportional to the simulated time.

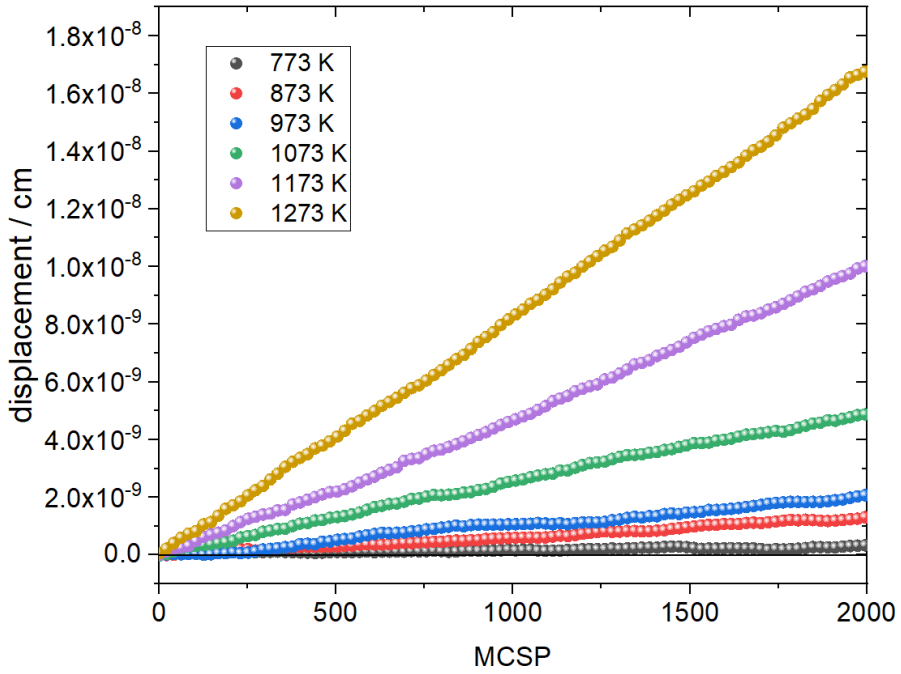

Figure 10 Displacement of oxide ions in the electric field for BZO10 with $\beta = 0.5$, including the vehicle mechanism. Displacement is shown depending on the number of Monte Carlo steps per particle (MCSP) which is proportional to the simulated time.

References

[1] S. Eisele and S. Grieshammer, MOCASSIN: Monte Carlo for Solid State Ionics, Forschungszentrum Jülich GmbH & RWTH Aachen University, GitHub repository, 2020.

[2] S. Eisele and S. Grieshammer, J. Comput. Chem., 2020, 41(31), 2663.

[3] F.M. Draber, C. Ader, J.P. Arnold, S. Eisele, S. Grieshammer, S. Yamaguchi and M. Martin, Nat. Mater., 2020, 19(3), 338.

[4] Draber, F. M.; Denninger, J. R.; Müller, P. C.; Sommerfeld, I. K. and Martin, M., Adv. Energy Sustainability Res. 2021, 3, 2200007.

[5] F.M. Draber, Ionic Conductivity in Acceptor-Doped Barium Zirconate. PhD Thesis, Aachen, 2021.